Article

Developmental Cell

Single-Cell Analysis Uncovers Clonal Acinar Cell Heterogeneity in the Adult Pancreas

Graphical Abstract

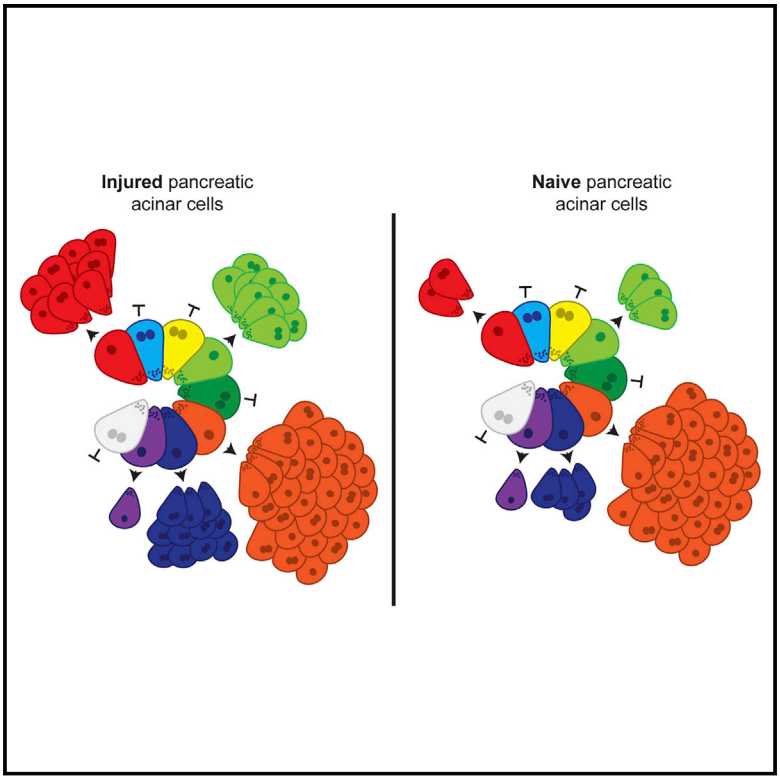

Authors

Damian Wollny, Sheng Zhao, Isabelle Everlien, ..., Wilko Weichert, Anna Marciniak-Czochra, Ana Martin-Villalba

Correspondence

a.martin-villalba@dkfz.de

In Brief

Wollny et al. show that acinar cells within the adult exocrine pancreas are heterogeneous. Most acinar cells exhibit a limited proliferative capacity or are binuclear and unable to divide. Assays by multicolor lineage tracing, organoid formation, and single-cell RNA-seq identify a minor subset of cells that retain proliferative activity long term.

Highlights

- Pancreatic acinar cells are heterogeneous in proliferative activity
- Only a minor subset of acinar cells retains proliferative activity long term
- By single-cell RNA-seq, STMN1 marks a proliferative acinar subpopulation
- Injury transiently activates proliferation and STMN1 expression in quiescent cells

Accession Numbers

GSE80032

Wollny et al., 2016, Developmental Cell *39*, 289–301
November 7, 2016
http://dx.doi.org/10.1016/j.devcel.2016.10.002

CellPress

Developmental Cell
Article

Single-Cell Analysis Uncovers Clonal Acinar Cell Heterogeneity in the Adult Pancreas

Damian Wollny,[1] Sheng Zhao,[1] Isabelle Everlien,[1] Xiaokang Lun,[1,5] Jan Brunken,[1] Daniel Brüne,[1] Frederik Ziebell,[1,2] Inna Tabansky,[3] Wilko Weichert,[4] Anna Marciniak-Czochra,[2] and Ana Martin-Villalba[1,6,*]
[1]Molecular Neurobiology, German Cancer Research Center (DKFZ), Im Neuenheimer Feld 280, 69120 Heidelberg, Germany
[2]Institute of Applied Mathematics, University of Heidelberg, 69120 Heidelberg, Germany
[3]Department of Neurobiology and Behavior, The Rockefeller University, 1230 York Avenue, New York, NY 10065, USA
[4]Institute of Pathology, Technical University of Munich, 81675 Munich, Germany
[5]Present address: Institute of Molecular Life Sciences, University of Zürich, 8057 Zürich, Switzerland
[6]Lead Contact
*Correspondence: a.martin-villalba@dkfz.de
http://dx.doi.org/10.1016/j.devcel.2016.10.002

SUMMARY

Acinar cells make up the majority of all cells in the pancreas, yet the source of new acinar cells during homeostasis remains unknown. Using multicolor lineage-tracing and organoid-formation assays, we identified the presence of a progenitor-like acinar cell subpopulation. These cells have long-term self-renewal capacity, albeit in a unipotent fashion. We further demonstrate that binuclear acinar cells are terminally differentiated acinar cells. Transcriptome analysis of single acinar cells revealed the existence of a minor population of cells expressing progenitor markers. Interestingly, a gain of the identified markers accompanied by a transient gain of proliferation was observed following chemically induced pancreatitis. Altogether, our study identifies a functionally and molecularly distinct acinar subpopulation and thus transforms our understanding of the acinar cell compartment as a pool of equipotent secretory cells.

INTRODUCTION

Life on earth evolved in the form of single-celled organisms. The "division of labor" by multiple cell types, however, provided an evolutionary benefit of multicellularity and the increase in cell-type diversity among metazoans (Arendt, 2008). The cellular diversity is at the heart of every multicellular organism. Yet, the definition of a cell type, although representing the basic building block of multicellular life, is surprisingly ill defined up to this day (Trapnell, 2015). Historically, most novel cell types have been defined on the basis of morphological differences as exemplified by the cell types in the pancreas.

The cell types within the pancreas can be divided into two classes: endocrine and exocrine cells. Endocrine cells, such as α or β cells, are hormone-producing cells responsible for the regulation of blood sugar homeostasis. The exocrine pancreas is responsible for producing and secreting large amounts of digestive enzymes into the digestive tract and entails ductal, acinar, and centroacinar cells. Exocrine acinar cells are "protein factories" which produce more proteins than any other adult cell type and make up the vast majority of all pancreatic cells (Logsdon and Ji, 2013). Although acinar cells are classified as a single cell type, the presence of mono- and binuclear cells was already reported in rats in the 1920s (Dolley, 1925) and later in the mouse (Ge and Morgan, 1990). However, whether this morphological feature is present in humans and whether it accompanies a different function has to date remained unexplored. Thus, assays probing functional differences might be needed to reveal novel cell types. An archetypical example of the discovery of a novel cell type by function was the discovery of stem cells in the murine bone marrow (Becker et al., 1963). The authors demonstrated that a single cell is capable of forming nodules on the spleen of recipient mice containing several cell types by taking advantage of radiation-induced chromosomal abnormalities that "barcode" the cellular progeny (Becker et al., 1963).

We aimed to use a similar approach whereby we can define functionally distinct acinar subpopulations on the single-cell level. By probing acinar heterogeneity using organoid-formation assays, multicolor lineage tracing, and single-cell RNA sequencing (RNA-seq), we discover progenitor-like acinar cells. This acinar subpopulation is source of new acinar cells during homeostasis and ultimately produces terminally differentiated, post-mitotic binuclear acinar cells revealing clonal heterogeneity among acinar cells.

RESULTS

An Acinar Subpopulation Forms Organoids In Vitro

Stem/progenitor cells of various organs have been described to have the unique capacity to form organoids under 3D culture conditions (Sasai, 2013). Thus, we tested whether progenitor-like acinar cells with organoid-forming capacity exist within the exocrine pancreas. To this end, we isolated acinar cells and plated them at a 500-cell density. Acinar cells gave rise to organoids that morphologically resembled organoids from other organs (Figure 1A and Movie S1). Between days 8 and 10 after plating, these acinar-derived organoids attached to the bottom of the well and frequently formed duct-like structures (Figure 1A and Movie S2). By day 5 post isolation, all acinar cells undergo a transition known

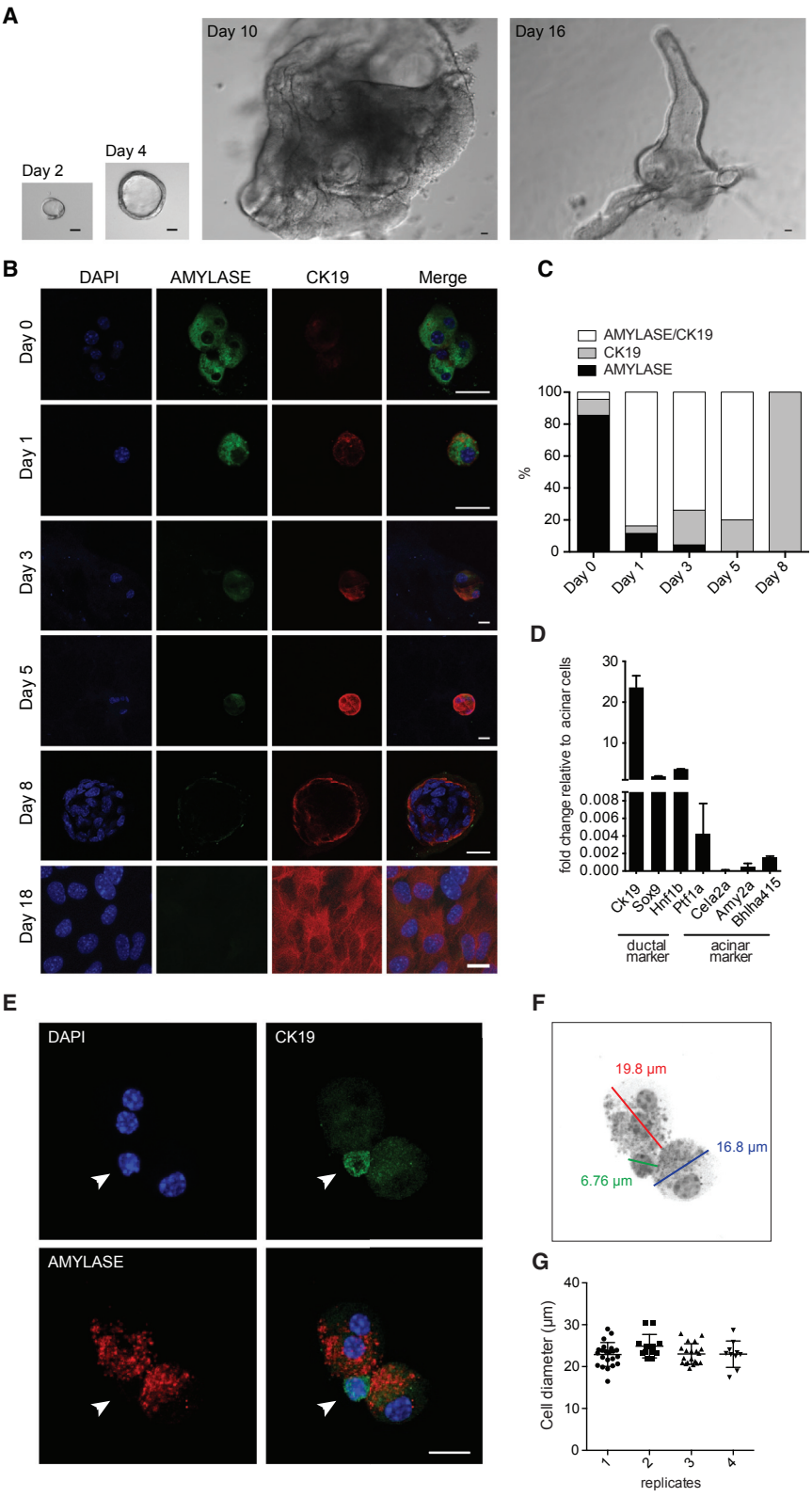

Figure 1. Acinar Cells Form Organoids In Vitro

(A) Representative examples of morphological transformation of acinar cell-derived organoid cultures over time. Scale bars, 20 µm.

(B) Amylase and CK19 expression analysis at various time points of organoid formation after acinar cell isolation. Scale bars, 20 µm.

(C) Quantification of cells expressing amylase and CK19 as assessed by immunofluorescence (n = 246 cells).

(D) qPCR analysis of acinar and ductal markers 7 days after isolation. Fold change over freshly isolated acinar cells is presented (n = 2). Data represent mean ± SD.

(E) Immunofluorescence staining of amylase and CK19 confirming acinar and ductal identity after cell isolation. Arrowheads indicate duct cells. Scale bar, 10 µm.

(F) Measurements of acinar and ductal cell diameter after isolation.

(G) Quantification of the cell diameter of all cells that gave rise to organoids after handpicking of acinar cells. 1–4 denote biological replicates.

See also Figure S1.

as acinar-to-ductal metaplasia as indicated by gained expression of ductal markers such as CK19 and a cuboidal epithelial shape at later times after plating (Figures 1B–D). Organoid formation by exocrine ductal cells has been previously reported (Huch et al., 2013; Jin et al., 2013). The purity of the organoid-forming cells was additionally checked by cell size to exclude that organoids derived from duct cells contaminating the acinar pool. Acinar cells are thrice as big as ductal cells, and this trait can be used to distinguish the two populations. Every organoid-forming cell exhibits the size of an acinar cell, which are clearly distinguishable from ductal cells (Figures 1E and 1F; Movie S1).

Yet, the question remained whether all acinar cells are able to form organoids. To assess both the organoid-formation capacity and the mitotic rates of acinar cells in the organoid-formation assay, we purified acinar cells from adult mice in which the histone H2B is genetically tagged with an mcherry fluorophore. With this tool at hand we could microscopically track the number of nuclei at any time during organoid formation. Quantification of mitotic activity following plating 500 acinar cells per well revealed that only a subpopulation of acinar cells was able to form organoids (Figure 2A). Surprisingly, isolated single acinar cells were unable to undergo more than one round of mitosis and did not proceed to form organoids (Figures 2A and S1A). To exclude that cell dissociation inhibited organoid formation of isolated acinar cells, we added the ROCK inhibitor Y-27632 to the culture medium

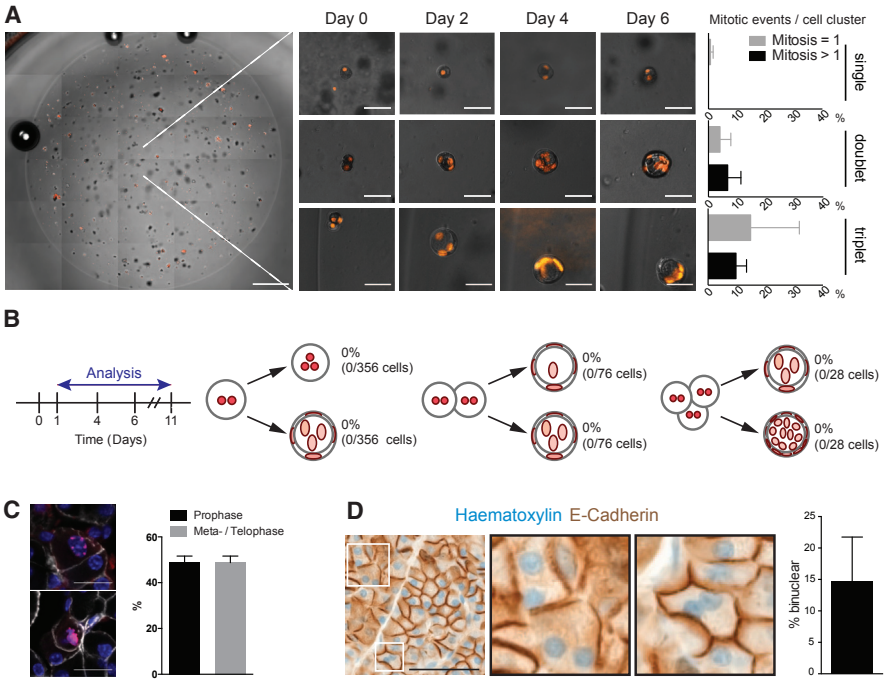

Figure 2. Proliferative Heterogeneity among Acinar Cells In Vitro

(A) Representative image of spontaneously formed organoids 0–6 days after isolation of adult pancreatic cells. Five hundred cells isolated from H2B-mcherry mice were plated in Matrigel and the rate of divisions from single cells, doublets, or triplets at day 0 was followed over a period of 11 days. Representative pictures of mitotic events of single cells (top row), doublets (middle row), and triplets (bottom row) are shown. Quantification of number of mcherry$^+$ nuclei is plotted on the right of the respective row. n = 1,899 cell clusters from three mice. Data represent means ± SD. Scale bars, 500 μm (overview) and 50 μm (close-ups).

(B) Quantification of mitotic events of binuclear acinar cells after culture of 500 acinar cells were isolated from adult H2B-mcherry mice.

(C) (Left) Representative confocal images showing pH3$^+$ (red), E-cadherin (white), and DAPI (blue) upon injury. The upper image depicts an acinar cell in prophase, whereas the lower image depicts a cell in meta-/telophase. (Right) Quantification of dividing acinar cells in pro- and metaphase was performed from three mice. Data represent mean ± SD. Scale bar, 20 μm.

(D) E-cadherin staining of paraffin-embedded human pancreatic sections reveals binuclear acinar cells. Hematoxylin was used for nuclear counterstaining. Scale bar, 50 μm. Insets: magnification of human binuclear acinar cells. Quantification (right) was performed from 15 patients. Data represent means ± SD.

See also Figure S2.

(Watanabe et al., 2007). Although we observed a significant survival advantage of single acinar cells treated with ROCK inhibitor, no single acinar cell divided more than once (Figures S1E and S1F).

Multiple mitotic events and subsequent organoid formation were exclusively observed in acinar doublets, triplets, and higher order clusters of acinar cells (Figures 2A and S1B–S1D). Hence, at least two acinar cells in contact are required to initiate organoid formation accompanied by more than one mitotic event. To test whether two acinar cells in direct contact were sufficient for organoid formation, we handpicked 682 acinar doublets and cultured them as single doublets per well. We observed organoid formation by 5% ± 2% acinar doublets, demonstrating that a "supporting" acinar cell is not only necessary but also sufficient for organoid formation (Figure S1G). Every cell in the examined doublets was an acinar cell, as assessed by size discrimination (Figure 1G). Assessment of functional differences among the two cells remains subject of future studies. Thus, similar to progenitors from other tissues, a subpopulation of acinar cells is able to form organoids once in direct cell-cell contact with other acinar cells.

Binuclear Acinar Cells Do Not Divide

The analysis of the proliferative behavior of single acinar cells revealed that without a supporting acinar cell, only a minor number of them would divide (Figure 2A). These isolated, single cells were able to divide only once and gave rise to binuclear acinar cells (Figure 2A). Furthermore, this analysis shows that binuclear cells arise by division of a mononuclear cell and not by cell fusion. The existence of binuclear acinar cells in the pancreas has been previously described in rats and mice, yet functional differences between mono- and binuclear cells remain elusive (Dolley, 1925; Ge and Morgan, 1990). The organoid-formation assay reveals that binuclear acinar cells are unable to divide, independent of the initial cluster size (Figure 2B). Next, we quantified dividing mono- and binuclear acinar cells in vivo by immunofluorescence staining of phospho-histone H3 (pH3) and E-cadherin (Figure S2). For the quantitative assessment, cerulein was injected into mice to induce pancreatitis and thereby increase the turnover rate of the acinar compartment to obtain a reasonable number of dividing cells in an otherwise highly quiescent tissue such as the pancreas (Fukuda et al., 2011; Nagashio et al., 2004). Although binuclear acinar cells make up almost half of all acinar cells in the pancreas (Figure S2A), pH3 exclusively marked dividing mononuclear acinar

cells while no difference regarding cell death was observed (Figures 2C and S2B). Distinction between binuclear and mononuclear cells would be difficult at late stages of mitosis after the nuclear envelope has disassembled and the two genomes of binucleated cells have already congressed into a common single spindle. Therefore, we additionally checked the mitotic stages in pH3-labeled cells. We scored pH3-positive cells at very early stages of mitosis as indicated by speckled staining (Figure 2C). While we did detect pH3-positive cells with single nuclei in these early mitotic stages, we did not detect a single binucleated cell at this time, indicating that binucleated cells do not enter into M phase (Figure 2C). The same was observed during homeostasis, albeit with considerably lower numbers of mitotic cells (Figure S2C). Together, these data indicate that binuclear acinar cells represent a post-mitotic state.

Next, we examined tissue sections from human pancreas to assess whether binuclear acinar cells also exist in the human pancreas. To this end, pancreatic tissue samples from 15 different human individuals were examined. These samples did not show any pathological signs. Importantly, binuclear acinar cells represented up to 15% of acinar cells, which is a previously neglected feature in the human pancreas and expands the relevance of our findings beyond rodents (Figure 1D). Taken together, our analysis reveals that binuclear acinar cells represent a distinct subpopulation of post-mitotic acinar cells, adding to the acinar cell diversity in mice and humans.

Multicolor Lineage Tracing Reveals Proliferative Heterogeneity among Acinar Cells

Next, we tested whether the proliferative heterogeneity among acinar cells in vitro can also be observed in vivo. To decipher clonal heterogeneity among acinar cells over time, we used a multicolor lineage-tracing approach with the *CAGGS* promoter upstream of the brainbow1.0 construct as previously described (Livet et al., 2007; Tabansky et al., 2013). Upon Cre induction, dTomato-expressing cells gain multiple colors upon expression of cerulein or eYFP (Figure S3A). The rainbow transgenic mouse used here generates a higher color diversity than the similar confetti system (Snippert et al., 2010), thereby facilitating distinction of different acinar clones over time without the need for sparse labeling, which would require a greater number of animals. To ensure exclusive recombination of this construct in the acinar compartment we used the Nestin-CreERT2 line. Similar to the Ela-CreERT2 line, the Nestin promoter reliably induces Cre expression only in acinar cells of the pancreas (Carrière et al., 2011). Absence of Cre recombination in non-acinar pancreatic cells was additionally confirmed in our mouse line (Figure 3A). Of note, recombination was absent in duct, Langerhans, or centroacinar cells (Figure 3A). To estimate the number of distinct colors generated in the pancreas upon Nestin-CreERT2 recombination, we conducted image analysis of 2,430 computationally segmented acinar cells. Using supervised affinity propagation clustering, we identified 17 distinct colors represented at different frequencies (Figures S3B–S3E).

To determine the clonal expansion of acinar cells from adult mice, we induced the Cre recombinase by tamoxifen injection (time point = 0) and analyzed the pancreata at various time points after injection (DPI: days post injection). The nuclei of acinar cells displayed high fluorescence (Figure 3B), which we subsequently used to estimate the clone size. Notably, a large number of two-nuclei clones were observed at 1 DPI (Figure 3C). These cells primarily comprise binuclear acinar cells, since the vast majority of acinar cells do not divide in such a short time frame (Figures 3C and S3F) (Kong et al., 2011). Thus, the majority of acinar cells did not divide within the first day after induction. At 7 DPI the first clones with multiple nuclei appeared (Figure 3C). The fact that acinar cells are either mono- or binuclear indicates that clones with three or more nuclei derive from cells, which divided once or more times. At later time points (28 and 84 DPI) even larger clones were detected (Figure 3C). Yet, even at 84 DPI the majority of all cells did not divide, indicating that proliferation is confined to a progenitor-like subpopulation of acinar cells.

An Acinar Subpopulation Retains Long-Term Proliferative Capacity In Vivo

Next, we wanted to test whether the described progenitor-like acinar subpopulation maintains long-term proliferative capacity or whether most acinar cells would eventually start to proliferate after long tracing periods. Following 1 year of tracing, the overall clonal distribution was surprisingly similar to the distribution observed at shorter time points, indicating that the majority of cells did not divide (Figures 4A and 4B). Only a small proportion of cells gave rise to clones of unexpectedly large size (Figures 4A and 4B). The relatively high proliferation rate of this acinar subpopulation was surprising given the low overall proliferation rate of acinar cells in the adult pancreas (Magami et al., 1990). The proliferation rate of acinar cells from aged mice did not significantly deviate from the rate in young adult mice (Figure S3F). The presence of a broad color distribution among the larger clones and the absence of morphological abnormalities argues against fluorophore toxicity (Figure S3G). Notably, the labeled acinar cells did not give rise to endocrine or ductal cells even after long tracing periods (Figure S3H). This confirms the previously described unipotent lineage restriction of acinar cells (Desai et al., 2007).

As mentioned above, our multicolor system labels acinar cells with some colors more frequently than others (Figure S3E). The overrepresentation of certain colors raised the question as to whether some large clones arose by a "clone fusion" event. In this scenario cells of an overrepresented color would be more likely than cells of an underrepresented color to be in close proximity. Thus, few mitotic events would theoretically lead to the fusion of clones of the same color. In this case the large clones would be polyclonal and not the result of a functionally distinct acinar cell with high proliferative capacity. To obtain a quantitative estimate of how likely clone fusion occurred in our dataset, we measured the diameter of each large clone of a certain color at 365 DPI. Next, we asked how many times we found cells of this color in the measured distance at 1 DPI and calculated the clone fusion probability (Figures S4A and S4B). The probability was below 10% for most clones, indicating that these clones arose from a single cell with high probability (Figure S4B). Importantly, for some of these very large clones the clone fusion probability was 0 (Figure S4B, groups 6, 11, and 15). This analysis strongly indicates that most large clones arise from a single cell with very high likelihood and thus serves as a proof of principle for the proliferative heterogeneity among acinar cells.

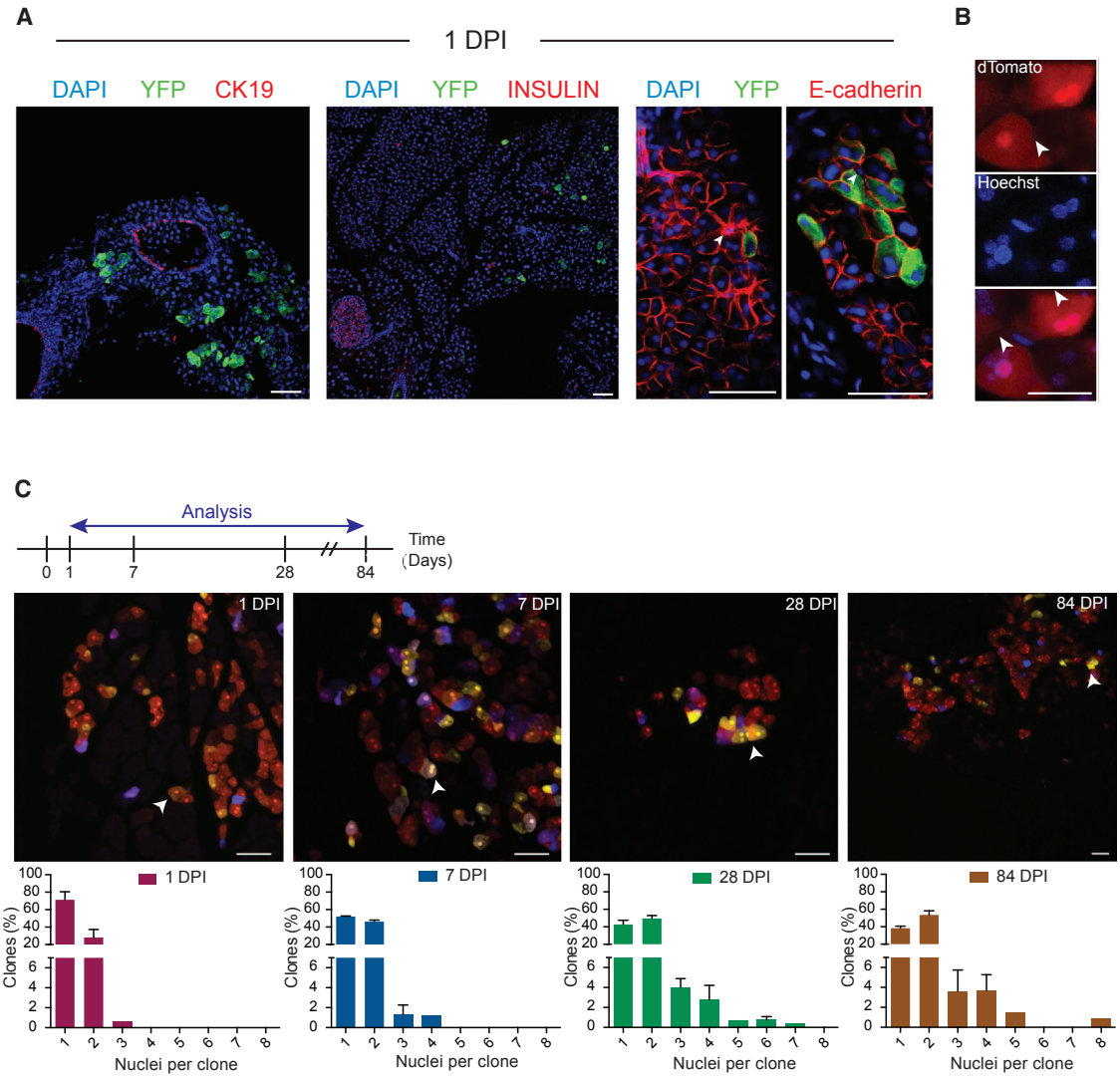

Figure 3. Clonal Tracing of Adult Acinar Cells Reveals Clonal Heterogeneity

(A) Nestin-CreERT2 rainbow2 mice at 1 DPI stained for YFP. Anti-YFP antibody detects all rainbow-induced clones. Anti-cytokeratin 19 (CK19) and anti-insulin staining was conducted to indicate duct cells and islets of Langerhans. Anti-E-cadherin staining was used to identify centroacinar cells (arrowheads). YFP was not expressed in duct, Langerhans, or centroacinar cells. n = 391 cells from two mice. Scale bars, 50 μm.

(B) Hoechst 33342 counterstaining indicates nuclear identity of bright subcellular structure upon rainbow2 expression (arrowheads). Scale bar, 25 μm.

(C) Quantitative analysis of the clone size distribution (fraction of clones with a certain number of nuclei) at the given time points after induction of the rainbow2 system. At 1 DPI, n = 885 clones from three mice were analyzed; at 7 DPI, n = 1,185 clones from five mice were analyzed; at 28 DPI, n = 681 clones from three mice were analyzed; at 84 DPI, n = 274 clones from three mice were analyzed. Arrowheads indicate representative examples of large clones found at the respective time points. Scale bars, 50 μm. Percentage of clones (bottom panels) was calculated for each biological replicate separately. Data represent mean ± SD.

See also Figure S3.

It is, however, possible that a uniform population of stochastically proliferating cells can give rise to large as well as small clones. To address this question, we conducted stochastic simulations by employing the Gillespie algorithm. Our results suggest that although a uniform population can explain the existence of a mixture of different clone sizes, the exact time dynamics as seen in the data cannot be reproduced (Figure S4C). In particular, the model predicts that the largest 1% of clones should have a bigger size than is observed in the data for the 28 and 84 DPI time points. Conversely, the largest 1% of clones should be smaller for 365 DPI based on a uniform model (Figure S4C). Thus, we can exclude the uniform population scenario using stochastic modeling.

Injury Induces Transient Activation of Quiescent Acinar Cells

Next, we wanted to address changes in clonal heterogeneity following a proliferative stimulus. Injection of cerulein induces proliferation of acinar cells (Fukuda et al., 2011; Nagashio et al., 2004). We hypothesized two models of clonal response

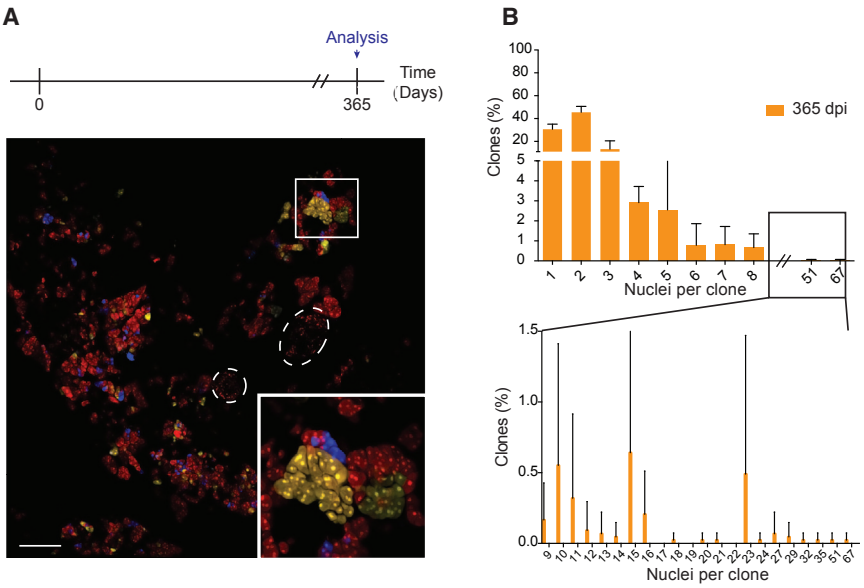

Figure 4. Clonal Analysis Uncovers an Acinar Subpopulation with Long-Term Proliferative Capacity

(A) Acinar cells are traced for a 1-year period post rainbow2 induction. Representative example of rainbow2-labeled acinar cells 1 year post label induction. Dashed circles indicate islets of Langerhans. Scale bar, 50 μm.

(B) Quantitative analysis of clones traced for 1 year following label induction (n = 1,283 clones from five mice). Data represent mean ± SD.

See also Figure S4.

to the injury: (1) the proliferative response to injury is confined to progenitor-like acinar clones that possess self-renewal capacity under homeostasis; and (2) a distinct population of acinar cells gains proliferative activity to compensate for the injury-induced cell loss (Figure 5A). To distinguish between these two models we combined a cerulein-induced injury model of acute pancreatitis with the multicolor lineage-tracing system. Cerulein was administered 48 hr after tamoxifen injection and rainbow2-labeled pancreata were analyzed at 28 days after tamoxifen injection (Figure 5A). This time point allows reliable detection of self-renewing clones in homeostasis (Figure 3C).

Cerulein injection led to a marked proliferative reaction including duct maker expression in the pancreas (Figure S5). Accordingly, injury-induced clonal expansion led to a significant increase in average clone size after 28 DPI compared with acinar clones in naive animals (Figures 5B and 5C). Interestingly no increase in maximum clone size was observed, suggesting that the injury increases the number of proliferating clones without altering the division rate of clones that are proliferating under homeostatic conditions (Figure 5C). To test whether the injury-induced proliferation is transient, we analyzed injured pancreata at 365 DPI. At this time no significant differences in average clone sizes between naive and injured mice were found, indicating the existence of a transient proliferative response (Figure 5D). Thus, injury-activated acinar cells do not seem to irreversibly convert into self-renewing cells. Furthermore, examination of sequential bromodeoxyuridine-ethynyldeoxyuridine (BrdU-EdU) labeling of the acinar compartment shows that in contrast to β cells, acinar cells that divided once have a higher probability of dividing a second time (Figures 5E and 5F).

Identification of Molecularly Distinct Acinar Subpopulation

Finally, we examined whether the functional heterogeneity we observed among acinar cells is also found at the molecular level. To this end, we aimed to perform single-cell RNA-seq of acinar cells. Acinar cells, however, produce massive amounts of RNAses in order to digest the nucleic acids within the diet (Barnard, 1969; Chirgwin et al., 1979). Thus, we had to develop a modified version of the SMART-seq2 protocol (Picelli et al., 2014) for library generation from tissues with high RNAse content (Experimental Procedures). Sequencing of libraries of 108 acinar cells resulted in total amounts of ~5 × 10^6 reads/cell and ~78% mapping rate similar to other published single-cell sequencing studies (Figures S6A and S6B) (Llorens-Bobadilla et al., 2015; Treutlein et al., 2014). Furthermore, we did not observe 3′ end sequencing bias and linear amplification as assessed by External RNA Control Consortium (ERCC) spike-in standards (Figures S6C–S6E).

When we compared the similarity of the acinar cells by Euclidean distance, we observed that the transcriptomes of individual acinar cells are strikingly similar (Figure 6A). However, we did observe acinar cells that differed considerably from the majority of cells (Figure 6B). The presence of these outliers was further confirmed by principal component analysis (PCA) (Figure S7A). These cells expressed markers of acinar cells (Figure 6C). Furthermore, the fact that we handpicked each acinar cell excludes cross-contamination by other cell types. We observed that 23% of all sequenced acinar cells expressed Nestin (Figure S6H), which is in excellent agreement with the recombination rate of the NesCreERT2 line in the pancreas (23%, Figure S3D). To identify possible transcriptional heterogeneity in the other main cluster of cells, we restricted our analysis to transcription factors expressed by acinar cells. Acinar lineage confined transcription factors such as *Ptf1a* and *Bhlha15* were robustly expressed in all profiled acinar cells, again confirming the acinar nature of the cells (Figure 6E, gray box). We identified two large clusters, which were mainly separated by early response genes such as *Jun*, *Fos*, and *Egr1*, and the stress response genes *Xbp-1* and *Atf3*, as well as *Klf6* (Figure 6E, black boxes).

Among the acinar cells, two outliers stood out (cell #40, cell #31; Figure 6B). Excitingly, Gene ontology (GO)-category analysis revealed enriched expression of genes related to cell-cycle activity and binding of chromatin in these cells (Figure 6D). Furthermore, genes implicated in chromatin remodeling, microtubule maintenance, and proliferation were also enriched in these outliers (Figure S7B). To validate the existence of this subpopulation in vivo, we sought a marker by comparing genes

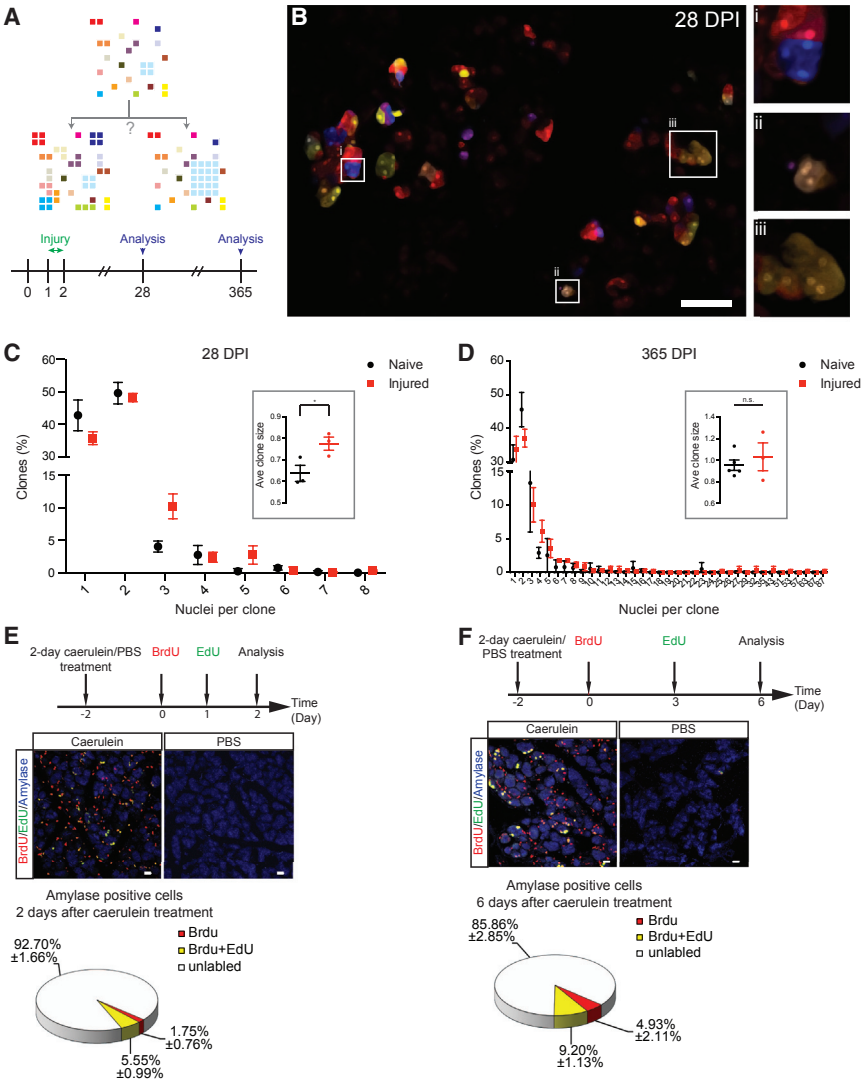

Figure 5. Injury Transiently Activates Quiescent Acinar Cells

(A) Experimental design and schematic illustration of potential changes of clone size distribution upon injury. Squares represent clonal clusters of acinar cells. Hypothesized outcome scenarios are clone size expansion of many previously dormant clones (left matrix) versus clone size expansion of the few clones actively proliferating under homeostatic conditions (right matrix). Pancreatic tissue was analyzed 28 and 365 days post injection.

(B) Representative illustration of clonal distribution 28 days after rainbow2 induction. Scale bar, 50 μm.

(C and D) Quantification of clone size distribution from naive and injured mice. For 28 DPI (C), n = 1,307 clones from three injured mice; for 365 DPI (D), n = 2,805 from three injured mice. Percentage of clones was calculated for each biological replicate separately. Data represent mean ± SD. Insets: average clone size comparison between naive and injured animals. Log_2 of clone sizes were calculated to obtain normal clone size distribution. Average clone size data are presented as mean ± SEM. *$p < 0.05$; n.s., not significant.

(E and F) Characterization of acinar cell proliferation and marker expression following cerulein-induced pancreatitis. Protocol for cerulein, BrdU, and EdU administration. Representative pie charts of corresponding quantification. At 2 days (E), n = 2,900 cells analyzed; at 6 days (F), n = 2,683 cells analyzed. Data represent means ± SD. Scale bar, 20 μm.

See also Figure S5.

differentially expressed between these two cells and the rest of the acinar cells. This analysis identified STMN1 as very highly expressed in both cells as opposed to others (Figure 6F). Interestingly, STMN1 was recently identified as a novel marker for early intermediate progenitor cells in the adult hippocampal subgranular zone (Shin et al., 2015) and a marker for progenitor cells in many other tissues (Cassimeris, 2002). We indeed observed expression of STMN1 in a subset of acinar cells by immunohistochemistry of adult pancreas (Figure 6G). Importantly, the Human Protein Atlas confirms the existence of an $STMN1^+$ acinar subpopulation in the human pancreas (Figure S7C). Thus, even if STMN1 was detected as an outlier by the single-cell transcriptome approach, immunohistochemistry for STMN1 reveals that the subset of $STMN1^+$ acinar cells is consistently found as a minor acinar population across species.

Interestingly, one of the STMN1-expressing outliers highly expressed *Sox9* whereas the other $STMN1^+$ acinar cells did not express it (Figure 6H). *Sox9* has been proposed to be a marker for progenitors of the exocrine pancreas (Furuyama et al., 2011). Although our single-cell transcriptome analysis reveals heterogeneous *Sox9* expression among the profiled cells, the $STMN1^+$ cells exhibited the highest *Sox9* expression level (Figure 6E, green box). To confirm this result we performed co-staining of STMN1 and Sox9. We found that the populations of acinar cells harbor both $STMN1^+/Sox9^+$ and $STMN1^+/SOX9^-$ cells, again validating our single-cell sequencing results (Figure 6I). In summary, the single-cell RNA data demonstrate that molecular heterogeneity underlies the previously observed functional heterogeneity and identifies a minor population of cells with an expression profile resembling proliferating progenitors.

Proliferating Acinar Cells Are $STMN1^+$ upon Injury

In agreement with the multicolor lineage-tracing data, the single-cell RNA-seq data reveal the existence of a small $STMN1^+$ acinar subpopulation with a proliferative transcriptional profile. Yet, our lineage-tracing data suggest that upon injury other acinar cells gain progenitor-like capacity to replenish the pool of acinar cells (Figure 5). We therefore tested whether acinar cells would transform into $STMN1^+$ progenitor-like acinar cells to acquire the capacity to proliferate. Immunohistochemical analysis of injured pancreata displayed a significantly higher number of $STMN1^+$ acinar cells (Figure 7A). Next, we tested whether $STMN1^+$ acinar cells are the source of new acinar cells upon injury. To this end we co-stained the injured tissue for STMN1 and the proliferation

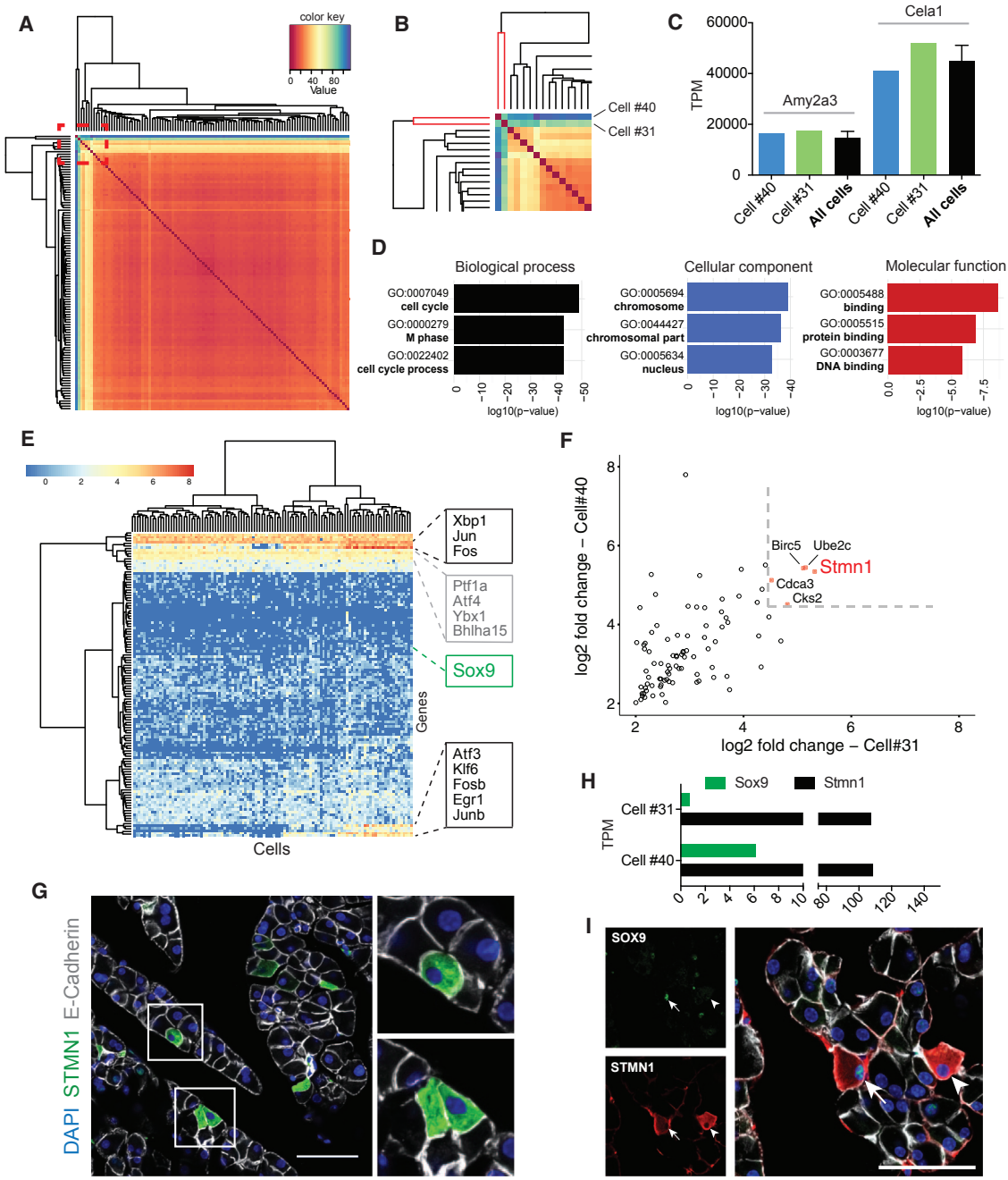

Figure 6. Single-Cell Sequencing Reveals Molecularly Distinct Acinar Subpopulations

(A) Heatmap indicating 108 single-cell transcriptome similarities measured by the Euclidean distance of the gene expression matrix.

(B) Magnification of heatmap inlet.

(C) Expression values of amylase (Amy2a3) and elastase (Cela1) for cell #40, cell #31, and the average (±SD) of all acinar cells. TPM, transcripts per million.

(D) GO category of genes highly expressed in cell #31 and cell #40.

(E) Heatmap illustrating heterogeneous expression of detected transcription factors in acinar cells.

(F) Log_2 fold change of differentially expressed genes in cell #40 and cell #31 over average expression of all acinar cells.

(G) Immunofluorescence staining confirming $STMN1^+$ acinar subpopulation in vivo. Scale bar, 50 μm.

(H) Expression values of STMN1 and Sox9 for cell #40 and cell #31. TPM, transcripts per million.

(I) Immunohistochemical analysis of STMN1 and Sox9 co-expression in acinar cells. Arrowhead indicates an $STMN1^+/Sox9^-$ acinar cell, whereas the arrow indicates an $STMN1^+/Sox9^+$ acinar cell. Scale bar, 50 μm.

See also Figures S6 and S7.

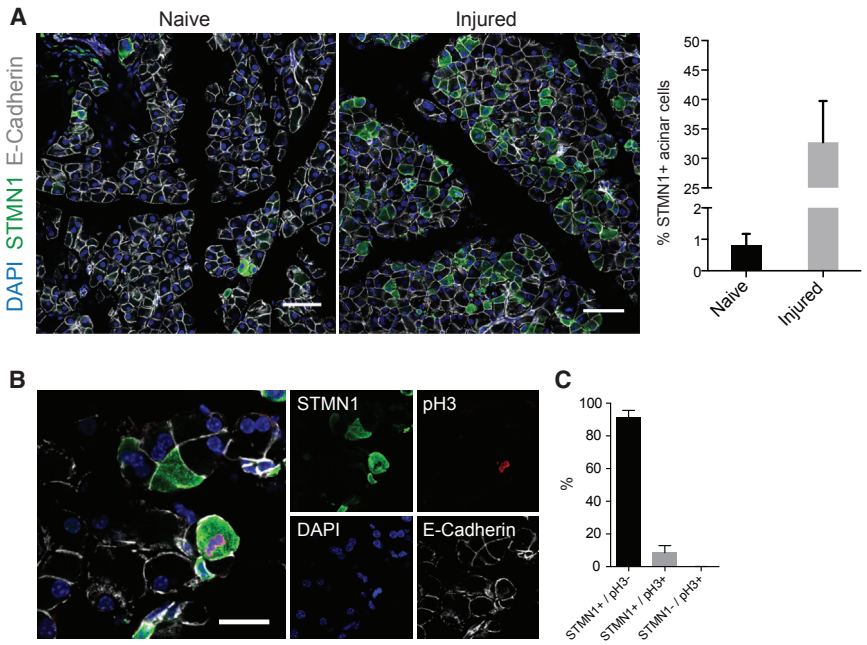

Figure 7. Proliferating Acinar Cells Are STMN1$^+$ upon Injury

(A) Immunohistochemical comparison of STMN1 expression in naive and injured mice. Injured mice were examined 4 days after cerulein injection. Data represent means ± SD. Scale bar, 50 μm.

(B) Representative images of proliferating acinar cells expressing high STMN1 levels. Scale bar, 20 μm.

(C) Quantification of STMN1 expression among proliferating acinar cells. Data represent mean ± SD for a total of 2,385 (91.38% ± 4.27%) STMN1$^+$/pH3$^-$, 187 (8.56% ± 4.32%) STMN1$^+$/pH3$^+$, and 2 (0.06% ± 0.05%) STMN1$^-$/pH3$^+$ cells from three mice.

marker pH3. In naive mice STMN1 was expressed by ~1% of the acinar cells (Figure 7). Upon injury, more than 30% of all acinar cells expressed STMN1 (Figure 7). We found that although only a minority of STMN1$^+$ acinar cells were actively cycling, almost all proliferating acinar cells were STMN1$^+$ (Figures 7B and 7C). This suggests that STMN1 marks progenitor-like acinar cells with the exclusive ability to give rise to new acinar cells upon injury. In addition, the fact that the vast majority of STMN1$^+$ acinar cells are not actively cycling argues against STMN1 being solely a proliferation marker. Most importantly, this finding links the transcriptome analysis to the lineage-tracing data, as at this time the amount of STMN1$^+$ cells and the clonal size increases upon injury.

DISCUSSION

The results obtained in the course of this study indicate that the decade-old notion of acinar cells representing a single homogeneous pool of cell is too simplistic. Our data suggest that the adult pancreas harbors fully differentiated acinar cells, from which a subset is able to self-renew for long periods of time to produce new acinar cells. This is majorly demonstrated by the lineage-tracing studies and the supporting modeling. To induce recombination of the brainbow construct required a high dose of tamoxifen, which could cause damage to the pancreas tissue and induce a proliferative state that otherwise would be absent under homeostatic conditions. However, using low tamoxifen dosage for a sparse-labeling protocol would have precluded detection of the very few large clones that are produced at the later time points (>84 DPI). Importantly, we show that a much more aggressive injury, as is the administration of cerulein, does not affect the number of large clones detected at 365 DPI. Thus, we can be sure that tamoxifen does not introduce any artifacts in our long-term lineage tracing and the resulting conclusions. The fact that we only have a minor population of large clones at the very late time points after tracing is in strong contrast to the uniform population model obtained from observations in the skin. In the skin, all cells start to proliferate with increasing time after tracing, and after 1 year a mixture of large and small clones is not observed but only large clones, leading to the conclusion that every cell is equipotent in terms of being able to divide (Clayton et al., 2007). In contrast, our data show that the overall distribution does not change with time, and we do detect a mixture of small clones and a few large ones. Altogether, we therefore conclude that these progenitor-like acinar cells are unipotent, yet they have the capacity for long-term self-renewal. Interestingly, similar mechanisms seem to drive the renewal of hepatocytes in the adult liver. Extensive lineage-tracing studies provide convincing evidence that adult hepatocytes are not multipotent (Yanger et al., 2014). However, an Axin2$^+$ subpopulation of hepatocytes was shown to be the source of new hepatocytes during homeostasis (Wang et al., 2015). Thus, both organs seem to harbor progenitor-like subpopulations among large pools of fully differentiated cells.

Another similarity between the pancreas and the liver is that both harbor binuclear cells (Guidotti et al., 2003). In the adult pancreas, binuclear cells were already observed in the 1920s (Dolley, 1925). However, it was unclear whether these cells are functionally different, which is likely why the community has largely ignored them. We demonstrate that these cells are terminally differentiated cells incapable of dividing and, most importantly, also exist in humans, indicating that generation of binuclear cells is an evolutionarily conserved trait. Binuclear cells have also been found in other tissues and are often associated with a decreased proliferative potential, as also reported here for acinar binuclear cells (Porrello et al., 2011; Rios et al., 2016). These cells are generated in the breast during lactation and disappear afterward (Rios et al., 2016). In the liver, binuclear cells disappear to give rise to two mononuclear cells to regenerate the liver after injury (Miyaoka et al., 2012). By contrast, we demonstrate that binuclear acinar cells do not divide upon injury. Furthermore, Axin2$^+$ hepatocyte progenitors are mostly mononuclear (Wang et al., 2015). Given these findings, it is tempting to speculate that a simple hierarchy might exist within these tissue compartments in which a mononuclear progenitor

ultimately produces terminally differentiated binuclear cells. However, more data are needed to unravel the complexity of the hierarchy as well as the differentiation kinetics.

Given the functional and morphological heterogeneity among acinar cells, we aimed to investigate whether this heterogeneity is based on molecular differences. With the help of single-cell RNA-seq we uncovered an acinar subpopulation expressing STMN1, also known as Stathmin or OP18. STMN1 is expressed by every dividing cell, but not every STMN1-positive cell divides (only ~10% of labeled cells). Thus, it is not merely a proliferation marker. This marker was also found to be expressed by progenitor cells of the dentate gyrus in the adult brain by a similar unbiased single-cell transcriptome analysis (Shin et al., 2015). Furthermore, STMN1 is expressed in progenitors of a variety of organs (Cassimeris, 2002). In addition, the number of STMN1-positive cells during homeostasis was definitely higher than the number of proliferating cells during homeostasis. Interestingly, we were able to confirm that STMN1 is expressed in a small population of acinar cells in humans (Uhlen et al., 2015). In mouse acinar cells STMN1 was expressed by 1% of the acinar cells. This percentage perfectly reflects the numbers found in the single-cell transcriptome analysis. Interestingly, this also roughly matches the amount of cells that would be producing the large clones found at 1 year after labeling.

We, moreover, found that one of the STMN1$^+$ cells expressed the progenitor marker Sox9. Sox9 is regarded as one of the pioneering factors in adult epidermal stem cells (Adam et al., 2015). Moreover, Sox9 is highly expressed in pancreatic duct cells (Seymour et al., 2007). It was previously proposed as a marker for progenitors of the exocrine pancreas based on a lineage-tracing study demonstrating that Sox9$^+$ duct cells give rise to acinar cells (Furuyama et al., 2011). However, an independent study could not confirm these results, leading to controversy within the field (Kopp et al., 2011). One possible explanation offered by our single-cell RNA-seq analysis is that Sox9 is expressed at very low levels in a small subset of acinar cells. High tamoxifen concentrations would label Sox9$^+$ acinar cells. Thus, differences in tamoxifen dosages used in different studies could potentially account for the contradictory results by previous studies.

Additionally our lineage-tracing data demonstrate that acinar cells outside the pool respond to the proliferative stimulus and not just the small subpopulation that mediates homeostatic turnover. It was previously described that acinar cells display marked plasticity upon injury (Puri et al., 2015; Puri and Hebrok, 2010; Ziv et al., 2013). Based on these observations, the concept of facultative stem cells was proposed for the adult pancreas (Kong et al., 2011; Yanger and Stanger, 2011). Interestingly, there was no detection of a specialized proliferative subpopulation within β cells in the endocrine pancreas (Teta et al., 2007). Using sequential thymidine analog treatment (chlorodeoxyuridine/iododeoxyuridine), the authors showed that β cells that undergo one round of proliferation are not more likely to divide again than β cells that have not recently divided. This result is in agreement with experiments performed using an H2B-GFP label retaining assay (Brennand et al., 2007). We were able to show that in contrast to β cells, acinar cells that gain the ability to proliferate upon exposure to cerulein would have a higher probability to divide again. Along this line, we observed marked upregulation of STMN1 in acinar cells upon injury. This indicates a transient acquisition of non-proliferative acinar cells into progenitor-like acinar cells in order to compensate for the injury-induced cell loss. Further analysis of acinar cells on the single-cell level will unravel the full cellular heterogeneity. It will be interesting to uncover the hierarchical relationship among the acinar cell types to complete our understanding of the adult pancreas.

EXPERIMENTAL PROCEDURES

Primary Human Tissue Samples

All human tissue samples were obtained with written informed consent under protocols approved by the review board of the Medical Faculty of the University of Heidelberg (Heidelberg, Germany).

Mice

C57BL/6N mice were purchased from Charles River Laboratories. B6(D2)-Tg(CAG-Brainbow1.0)2Eggn/J (CAG-Rainbow2) were kindly provided by Dr. Kevin Eggan (Tabansky et al., 2013) and crossed with B6.Cg-Tg(Nes-cre/Esr1)GSc (Nes-CreER^{T2}). For lineage-tracing experiments, mice were used at 12 weeks of age. H2B-mcherry mice were a kind gift of Dr. Jan Ellenberg. Animals were housed in the animal facilities of the German Cancer Research Center (DKFZ) on a 12-hr dark/light cycle and had free access to food and water. All animal experiments were performed in accordance with institutional guidelines of the German Cancer Research Center and were approved by the Regierungspräsidium Karlsruhe (Project Numbers G193/13, A8-15), Germany.

Tissue Preparation for Rainbow2 Imaging

To induce rainbow2 colors, we intraperitoneally injected adult rainbow2 mice with 100 μL of 10 mg/mL tamoxifen (Sigma-Aldrich) twice daily for 5 consecutive days. Despite the high tamoxifen concentration, we observed very variable labeling efficiency from mouse to mouse. At given time points the mice were perfused with Hank's balanced salt solution (HBSS) at room temperature following 4% ice-cold paraformaldehyde (PFA). The pancreas was extracted, adipose tissue carefully removed, and the pancreas post-fixed for 15 min in 4% PFA on ice. Afterward the pancreas was transferred to 30% sucrose in PBS and incubated at 4°C until the tissue settled on the bottom of the vessel. The pancreas was embedded in OCT compound (Sakura) and stored at −20°C overnight. Tissue sectioning was performed using a CM 1950 Cryomicrotome (Leica) with the cryochamber and specimen head at −20°C. Section thickness for time points 1, 7 28, and 84 DPI was 20 μm and for time point 365 DPI, 50 μm. Four consecutive sections were collected on each glass slide, mounted with Fluoromount G (eBioscience), and directly imaged under a TCS SP5 confocal microscope (Leica).

Confocal Analysis of Rainbow2 Pancreas Sections

Images were acquired as xyz stacks at a 1,024 × 1,024 pixel resolution. z Planes of images were quantified separately. For representation, maximum projection of z planes was used. For fluorophore excitation, the following settings were used: dTomato (helium-neon laser 561 nm; 1 mW, emitted photons collected between 572 and 686 nm), cerulein (argon multiline laser 458 nm, 100 mW, emitted photons collected between 464 and 504 nm), eYFP (argon multiline laser 514 nm, 100 mW, emitted photons collected between 522 and 576 nm). Tunable spectral photomultiplier tubes were used as detectors. Clones were discriminated by color composition, and clone size was determined by counting of nuclei within a clone.

Acinar Cell Isolation and Culture

Mice were perfused with 20 mL of HBSS (Gibco), and the pancreas was extracted and adipose tissue removed. Four solutions were prepared, including D solution (1 mg/mL Collagenase Type CLS IV supplemented with 0.25% BSA [Sigma-Aldrich]), R solution (1% BSA dissolved in PBS), C solution (4% BSA in PBS), and I solution (0.1% BSA in PBS). The tissue was chopped into small pieces and incubated in 10 mL of D solution at 37°C for 30 min. The digestion

product was filtered through a 70-μm cell strainer (islets of Langerhans were thereby removed). Ten milliliters of R solution was pipetted on the cell strainer. A quarter of the filtered cell suspension was gently transferred on top of 6 mL of C solution to achieve layer separation of the liquids. Acini were spun down at 50 × *g* for 2 min and washed with C solution and I solution successively. Purified acini were treated with 2 mL of Accutase (Sigma-Aldrich) for 5 min to acquire acinar cell suspension containing single cells and clusters of acinar cells.

Single acinar cells or acinar doublets isolated from H2B-mcherry mice were handpicked using heat-pulled glass capillaries (beveled at 30°C with an inner diameter of approximately 75–100 μm) and transferred to 20 μL of Matrigel, which was kept unpolymerized on ice. Cell viability and correct cell number were assessed immediately afterward by fluorescence microscopy.

For 500 acinar cell experiments, the mixture was pipetted as drops in selected cell-culture plates or dishes and incubated at 37°C for 20 min before the addition of culture medium. The cells were cultured for 11 days and imaged on days 0–4 as well as on days 6 and 11.

The medium used to culture pancreatic cells was composed of a 1:1 mixture of DMEM high glucose (Sigma-Aldrich) and Ham's F-12 Nutrient Mix, GlutaMAX (Gibco), with the supplementary of 2% (v/v) B27 Serum-Free Supplement (Gibco), 1% (v/v) N-2 Supplement (Gibco), 20 ng/mL rHu epidermal growth factor (Promokine), 20 ng/mL human fibroblast growth factor 2 (ReliaTech), and 1% penicillin-streptomycin (100 units/mL, Gibco). Cells were cultured at 37°C and the medium was refreshed every third day. Organoid imaging was conducted using a Cell Observer (Zeiss).

Cerulein Treatment

Acute pancreatitis was induced as previously described (Carrière et al., 2011). In brief, adult mice were intraperitoneally injected with cerulein (Sigma-Aldrich) in PBS (50 μg/kg body weight) hourly for 7 hr on 2 consecutive days. The last injection on day 2 was defined as time point 0 and mice were euthanized 28 or 365 days later.

Acinar Proliferation Measurements Using EdU Incorporation

Acinar cell proliferation in 8-week-old mice was assessed by intraperitoneal injection of 100 μg of EdU per gram body weight once per day on 3 consecutive days. One day after the last injection, the mice were euthanized and perfused with HBSS. Acinar cells were isolated as previously described and stained for EdU using the EdU click-iT kit (Life Technologies). For fluorescence-activated cell sorting analysis of acinar cells, 50,000 events were measured and the gates for exclusion of dead cells, doublets, and EdU-positive cells were set as shown in an EdU-negative control.

Proliferation and Clonal Analysis of Pancreas Regeneration with BrdU and EdU

Pancreatitis was induced using cerulein as described above. After the last injection, cerulein-treated mice and PBS-treated control mice were injected intraperitoneally with BrdU (100 mg/kg). BrdU incorporated was detected by immunofluorescence using the rat anti-BrdU antibody (AbD Serotec, 1:250). Between specimen rehydration and blocking, slides were treated with 2 M HCl at 37°C for 30 min to denature the DNA and expose the BrdU. Samples were then rinsed in 100 mM Borate Buffer for 10 min at room temperature and washed six times (5 min for each item) in PBS containing 0.2% Triton X-100. Immunostaining continued with blocking and primary antibody application as indicated in Supplemental Experimental Procedures. EdU was detected using the Click-iT EdU Alexa Fluor 647 Flow Cytometry Assay Kit before applying the secondary antibody for BrdU staining.

Single-Cell RNA-Seq

The single-cell RNA-seq library preparation protocol was based on the SMART seq2 protocol (Picelli et al., 2014) with following modifications.

Acinar cells were isolated as described in the section Acinar Cell Isolation and Culture and resuspended in DPBS without Ca^{2+} and Mg^{2+} (PAN-Biotech). Cells were collected in a volume of 0.5 μL and transferred to a reaction tube containing 4 μL of 6 M guanidine-HCl (Sigma-Aldrich), 0.1% (v/v) Triton X-100 (Sigma-Aldrich) and 1% (v/v) 2-mercaptoethanol (Sigma-Aldrich). The tube was immediately transferred into liquid nitrogen and kept there for the duration of cell collection. Next, 2.2× RNA SPRI beads (Beckman Coulter) were added directly to the lysis buffer and incubated for 5 min at room temperature. The beads were washed twice with 70% ethanol. Air-dried beads were resuspended in a solution containing 2 μL of H20, 1 μL of oligo(dT) primer, and 1 μL of dNTP Mix (primer and nucleotides used as in Picelli et al., 2014). Twenty-four cells contained ERCC Spike-In RNAs (1:10,000; Mix2, Ambion) Mix in addition to primer and nucleotides. Beads were incubated for 3 min at 72°C, and reverse transcription and PCR (19 cycles) were performed as described by Picelli et al. (2014). PCR product was cleaned up using 0.8× DNA SPRI beads (Beckman Coulter), and air-dried beads were resuspended in 15 μL of H_2O. The quality of cDNA library was assessed for each cell on a high-sensitivity DNA Bioanalyzer chip. Subsequent steps (tagmentation, amplification, multiplexing) were done as previously described (Llorens-Bobadilla et al., 2015). The DKFZ Genomics and Proteomics Core Facility conducted sequencing on an Illumina HiSeq2000 sequencer (paired-end 100 bp).

Single-Cell RNA-Seq Data Analysis

The single-cell RNA-seq data accession number is GEO: GSE80032; single-cell analysis uncovers clonal heterogeneity in the adult exocrine pancreas, http://www.ncbi.nlm.nih.gov/geo/query/acc.cgi?acc=GSE80032.

In total, we carried out single-cell RNA-seq on 108 acinar cells. Data analysis steps are described as follows.

Read Trimming and Mapping

Quality of raw reads was checked by FASTQC (http://www.bioinformatics.babraham.ac.uk/projects/fastqc/). Before alignment, adapter sequences in raw reads were trimmed by Btrim64 (http://graphics.med.yale.edu/trim) (Kong, 2011). Trimmed reads were mapped to mouse genome (ENSEMBL Release 80) using STAR_2.4.2a. Genome-mapping results were visualized by using Integrative Genome Viewer (www.broadinstitute.org/igv/).

RNA-Seq Data Quality Metrics

RNA-seq data quality metrics of each cell, including total reads, transcriptome mapped reads, and transcriptome mapped rate was calculated by picard-tools-1.123 (https://broadinstitute.github.io/picard/) as shown in Table S1.

Gene Expression Matrices

Gene expression matrices were generated as previously described (Llorens-Bobadilla et al., 2015; Shalek et al., 2013, 2014) with slight modifications. In brief, the expression level of each gene was quantified in units by transcript per million (TPM) using RSEM 1.2.21 (Li and Dewey, 2011) with bowtie2-2.2.6 using default parameters. To compare expression levels of different genes across samples, we performed an additional TMM (trimmed mean of M-values) normalization on TPM using Trinity (Haas et al., 2013) (http://trinityRNA-seq.github.io/) based on edgeR (Robinson and Oshlack, 2010) (abbreviated TMM-TPM). The purpose of this normalization is to account for differences in total cellular RNA production across all cells.

Validation of Single-Cell RNA-Seq Data Using ERCC Spike-In Controls, Technical Replicates, and Population RNA-Seq Data

We assessed the quality of single-cell RNA-seq data by comparing the results with known quantities of 92 ERCC spike-in RNA transcripts. In brief, 92 ERCC spike-in RNA transcripts were randomly add to 19 single cells when preparing the library. Expression levels of 92 ERCC spike-in controls in these 19 cells were quantified in units of TPM by RSEM. The expression levels of ERCC spike-in determined by RNA-seq strongly correlated with the known input quantities (Figure S6C).

Principal Component Analysis

We developed custom R scripts based on the FactoMineR library (http://factominer.free.fr/) to perform PCA on gene expression matrices. PCA was performed on cells that passed quality control using all genes expressed in more than two cells and with a variance in $\log_2$ (TMM-TPM) across all single cells greater than 0.5. In total, 4,628 genes in 108 cells were used. Subsequently, genes with the highest correlation coefficient with one of the first three or four principal components were identified using the dimdesc function in FactoMineR. Hierarchical clustering was performed on cells and on the genes identified by PCA using Euclidean distance or correlation metric.

Gene Ontology Analysis

GO analysis was done using the DAVID database (v6.7) (Dennis et al., 2003).

Image Analysis

Cells from images of recombined NesCreERT2 rainbow2 mice were segmented using a modified version of the segmentation from Cervero et al.

(2013) implemented as a macro for the Fiji software. For each segmented cell the median RGB values and pixel coordinates were recorded and saved. The values were then imported into R and converted into the HSV color space. We decided to use the HSV color space because the two important variables for our analysis, hue and saturation, are distinct variables in this space. The brightness value was neglected since it might vary between experiments. Small cell fragments or larger cell conglomerates were discarded with manually set cutoff values. We then clustered the segmented cells based on the similarity of their hue and saturation values in a 2D scatter plot. For this purpose, we had to shift the hue values for all cells by 180° because our data showed dense coverage in the red hue values, which are located at the edges of our 2D plot, but had a gap in the blue hue values, located in the middle. To discover the number of colors in a bottom-up fashion, we decided to utilize a clustering algorithm that does not require a priori determination of the number of clusters. For this purpose we decided to use affinity propagation clustering (Frey and Dueck, 2007). The affinity propagation clustering algorithm defines a certain amount of colors (clusters) as well as an example cell for this color (exemplars) autonomously. However, in contrast to, e.g., the k-means clustering algorithm this algorithm simultaneously considers all cells to be potential exemplars for clusters. Thus, it does not require initially randomly defined exemplars to which the result is quite sensitive (Frey and Dueck, 2007). The number of clusters the algorithm detects depends on input preference values (q values). Depending on the q values we obtained a color range from 14 to 108 clusters. Next, we aimed to find out which cluster number most likely represents the true amount of colors. For this purpose we supervised the clustering. We examined the exemplars of each cluster by eye and clustered them according to their similarity. Although the number of clusters linearly increases as a function of the q values, our manual analysis showed that the number of supervised clusters saturates. We therefore considered the supervised cluster number at q = 0.5 to be closest to the true amount of colors we detect in our setup, since an even higher q value will be very unlike to provide more colors in the supervised clustering analysis.

Clone Fusion Probability Estimation

The coordinates of the cells are clustered into groups such that all elements in one group can be connected by a spanning tree with edges having (at most) the cutoff length. The cutoff length is defined by the maximum diameter of the largest clone we could find for each color. The resulting clusters, which consist of only one element, correspond to cells that cannot give rise to clones resulting from clone fusion. In contrast, cells within a cluster can form fused clones, and the maximum possible number of fused clones arising from a cluster is the integer quotient of the number of cells in the cluster and 2. For example: a cluster of seven cells can form at most three fused clones (two clones out of two cells and one clone out of three cells). An upper boundary for the probability that a cluster of cells is the result from clonal fusion is thus given by the ratio of the maximum number of clones that could potentially fuse to the total number of clones. This upper boundary therefore represents a ''worst-case scenario'' for any given clone fusion event.

ACCESSION NUMBERS

The single-cell RNA-seq data accession number reported in this paper is GEO: GSE80032.

SUPPLEMENTAL INFORMATION

Supplemental Information includes Supplemental Experimental Procedures, seven figures, one table, and two movies and can be found with this article online at http://dx.doi.org/10.1016/j.devcel.2016.10.002.

AUTHOR CONTRIBUTIONS

D.W. and A.M.V. conceived the study and designed the experiments. D.W., I.E., X.L., and J.B. performed the experiments. S.Z. performed computational analysis of the RNA-seq data. D.B., F.Z., and D.W. performed rainbow2 image analysis. I.T. was involved in establishing rainbow2 imaging experiments. F.Z. and A.M.C. performed statistical analysis and mathematical modeling. W.W. provided and stained human pancreatic samples. D.W. and A.M.V. wrote the manuscript.

ACKNOWLEDGMENTS

We thank Günther Schütz for the Nestin CreER^{T2} mouse line, Kevin Eggan for the rainbow2 mouse line, and Jan Ellenberg and Judith Reichmann for the H2B-mcherry mouse line. Support from the DKFZ Light Microscopy Facility and the DKFZ Genomics and Proteomics Core Facility is gratefully acknowledged. We further thank Stefanie Limpert, Katrin Volk, and Melanie Richter for genotyping of mouse lines. We also thank Dorothee Bornhorst for experimental help. Furthermore, we are thankful to Alex Shalek and Simone Picelli for advice while developing the single-cell RNA-seq protocol. We thank Jan Lohmann and Peter Angel for critical discussions. This work was supported by the German Cancer Research Center (DKFZ), the National Center for Tumor Diseases Heidelberg (NCT, IFP IV), and the German Research Foundation (DFG, SFB 873).

Received: August 9, 2016
Revised: September 30, 2016
Accepted: October 3, 2016
Published: October 27, 2016

REFERENCES

Adam, R.C., Yang, H., Rockowitz, S., Larsen, S.B., Nikolova, M., Oristian, D.S., Polak, L., Kadaja, M., Asare, A., Zheng, D., and Fuchs, E. (2015). Pioneer factors govern super-enhancer dynamics in stem cell plasticity and lineage choice. Nature *521*, 366–370.

Arendt, D. (2008). The evolution of cell types in animals: emerging principles from molecular studies. Nat. Rev. Genet. *9*, 868–882.

Barnard, E.A. (1969). Biological function of pancreatic ribonuclease. Nature *221*, 340–344.

Becker, A.J., McC, E.A., and Till, J.E. (1963). Cytological demonstration of the clonal nature of spleen colonies derived from transplanted mouse marrow cells. Nature *197*, 452–454.

Brennand, K., Huangfu, D., and Melton, D. (2007). All beta cells contribute equally to islet growth and maintenance. PLoS Biol. *5*, e163.

Carrière, C., Young, A.L., Gunn, J.R., Longnecker, D.S., and Korc, M. (2011). Acute pancreatitis accelerates initiation and progression to pancreatic cancer in mice expressing oncogenic kras in the nestin cell lineage. PLoS One *6*, e27725.

Cassimeris, L. (2002). The oncoprotein 18/stathmin family of microtubule destabilizers. Curr. Opin. Cell Biol. *14*, 18–24.

Cervero, P., Panzer, L., and Linder, S. (2013). Podosome reformation in macrophages: assays and analysis. Methods Mol. Biol. *1046*, 97–121.

Chirgwin, J.M., Przybyla, A.E., MacDonald, R.J., and Rutter, W.J. (1979). Isolation of biologically active ribonucleic acid from sources enriched in ribonuclease. Biochemistry *18*, 5294–5299.

Clayton, E., Doupé, D.P., Klein, A.M., Winton, D.J., Simons, B.D., and Jones, P.H. (2007). A single type of progenitor cell maintains normal epidermis. Nature *446*, 185–189.

Dennis, G., Sherman, B.T., Hosack, D.A., Yang, J., Gao, W., Lane, H.C., and Lempicki, R.A. (2003). Genome biology | full text | DAVID: database for annotation, visualization, and integrated discovery. Genome Biol. *4*, P3.

Desai, B.M., Oliver-Krasinski, J., De Leon, D.D., Farzad, C., Hong, N., Leach, S.D., and Stoffers, D.A. (2007). Preexisting pancreatic acinar cells contribute to acinar cell, but not islet β cell, regeneration. J. Clin. Invest. *117*, 971–977.

Dolley, D.H. (1925). The general morphology of pancreatic cell function in terms of the nucleo-cytoplasmic relation. Am. J. Anat. *35*, 153–197.

Frey, B.J., and Dueck, D. (2007). Clustering by passing messages between data points. Science *315*, 972–976.

Fukuda, A., Wang, S.C., Morris, J.P., IV, Folias, A.E., Liou, A., Kim, G.E., Akira, S., Boucher, K.M., Firpo, M.A., Mulvihill, S.J., and Hebrok, M. (2011). Stat3 and

MMP7 contribute to pancreatic ductal adenocarcinoma initiation and progression. Cancer Cell *19*, 441–455.

Furuyama, K., Kawaguchi, Y., Akiyama, H., Horiguchi, M., Kodama, S., Kuhara, T., Hosokawa, S., Elbahrawy, A., Soeda, T., Koizumi, M., et al. (2011). Continuous cell supply from a Sox9-expressing progenitor zone in adult liver, exocrine pancreas and intestine. Nat. Genet. *43*, 34–41.

Ge, Y.C., and Morgan, R.G. (1990). Changes in numbers of pancreatic acinar cell nuclei and in DNA content during raw soya flour feeding in mice. Am. J. Anat. *189*, 207–212.

Guidotti, J.E., Bregerie, O., Robert, A., Debey, P., Brechot, C., and Desdouets, C. (2003). Liver cell polyploidization: a pivotal role for binuclear hepatocytes. J. Biol. Chem. *278*, 19095–19101.

Haas, B.J., Papanicolaou, A., Yassour, M., Grabherr, M., Blood, P.D., Bowden, J., Couger, M.B., Eccles, D., Li, B., Lieber, M., et al. (2013). De novo transcript sequence reconstruction from RNA-seq using the Trinity platform for reference generation and analysis. Nat. Protoc. *8*, 1494–1512.

Huch, M., Bonfanti, P., Boj, S.F., Sato, T., Loomans, C.J.M., van de Wetering, M., Sojoodi, M., Li, V.S.W., Schuijers, J., Gracanin, A., et al. (2013). Unlimited in vitro expansion of adult bi-potent pancreas progenitors through the Lgr5/R-spondin axis. EMBO J. *32*, 2708–2721.

Jin, L., Feng, T., Shih, H.P., Zerda, R., Luo, A., Hsu, J., Mahdavi, A., Sander, M., Tirrell, D.A., Riggs, A.D., and Ku, H.T. (2013). Colony-forming cells in the adult mouse pancreas are expandable in Matrigel and form endocrine/acinar colonies in laminin hydrogel. Proc. Natl. Acad. Sci. USA *110*, 3907–3912.

Kong, Y. (2011). Btrim: a fast, lightweight adapter and quality trimming program for next-generation sequencing technologies. Genomics *98*, 152–153.

Kong, B., Michalski, C.W., Erkan, M., Friess, H., and Kleeff, J. (2011). From tissue turnover to the cell of origin for pancreatic cancer. Nat. Rev. Gastroenterol. Hepatol. *8*, 467–472.

Kopp, J.L., Dubois, C.L., Schaffer, A.E., Hao, E., Shih, H.P., Seymour, P.A., Ma, J., and Sander, M. (2011). Sox9+ ductal cells are multipotent progenitors throughout development but do not produce new endocrine cells in the normal or injured adult pancreas. Development *138*, 653–665.

Li, B., and Dewey, C.N. (2011). RSEM: accurate transcript quantification from RNA-Seq data with or without a reference genome. BMC Bioinformatics *12*, 323.

Livet, J., Weissman, T.A., Kang, H., Draft, R.W., Lu, J., Bennis, R.A., Sanes, J.R., and Lichtman, J.W. (2007). Transgenic strategies for combinatorial expression of fluorescent proteins in the nervous system. Nature *450*, 56–62.

Llorens-Bobadilla, E., Zhao, S., Baser, A., Saiz-Castro, G., Zwadlo, K., and Martin-Villalba, A. (2015). Single-cell transcriptomics reveals a population of dormant neural stem cells that become activated upon brain injury. Cell Stem Cell *17*, 329–340.

Logsdon, C.D., and Ji, B. (2013). The role of protein synthesis and digestive enzymes in acinar cell injury. Nat. Rev. Gastroenterol. Hepatol. *10*, 362–370.

Magami, Y., Azuma, T., Inokuchi, H., Kawai, K., and Hattori, T. (1990). Turnover of acinar cells in mouse pancreas. J. Gastroenterol. *25*, 514.

Miyaoka, Y., Ebato, K., Kato, H., Arakawa, S., Shimizu, S., and Miyajima, A. (2012). Hypertrophy and unconventional cell division of hepatocytes underlie liver regeneration. Curr. Biol. *22*, 1166–1175.

Nagashio, Y., Ueno, H., Imamura, M., Asaumi, H., Watanabe, S., Yamaguchi, T., Taguchi, M., Tashiro, M., and Otsuki, M. (2004). Inhibition of transforming growth factor β decreases pancreatic fibrosis and protects the pancreas against chronic injury in mice. Lab. Invest. *84*, 1610–1618.

Picelli, S., Faridani, O.R., Björklund, Å.K., Winberg, G., Sagasser, S., and Sandberg, R. (2014). Full-length RNA-seq from single cells using Smart-seq2. Nat. Protoc. *9*, 171–181.

Porrello, E.R., Mahmoud, A.I., Simpson, E., Hill, J.A., Richardson, J.A., Olson, E.N., and Sadek, H.A. (2011). Transient regenerative potential of the neonatal mouse heart. Science *331*, 1078–1080.

Puri, S., and Hebrok, M. (2010). Cellular plasticity within the pancreas- lessons learned from development. Dev. Cell *18*, 342–356.

Puri, S., Folias, A.E., and Hebrok, M. (2015). Plasticity and dedifferentiation within the pancreas: development, homeostasis, and disease. Cell Stem Cell *16*, 18–31.

Rios, A.C., Fu, N.Y., Jamieson, P.R., Pal, B., Whitehead, L., Nicholas, K.R., Lindeman, G.J., and Visvader, J.E. (2016). Essential role for a novel population of binucleated mammary epithelial cells in lactation. Nat. Commn. *7*, 11400.

Robinson, M.D., and Oshlack, A. (2010). A scaling normalization method for differential expression analysis of RNA-seq data. Genome Biol. *11*, R25.

Sasai, Y. (2013). Next-generation regenerative medicine: organogenesis from stem cells in 3D culture. Cell Stem Cell *12*, 520–530.

Seymour, P.A., Freude, K.K., Tran, M.N., Mayes, E.E., Jensen, J., Kist, R., Scherer, G., and Sander, M. (2007). SOX9 is required for maintenance of the pancreatic progenitor cell pool. Proc. Natl. Acad. Sci. USA *104*, 1865–1870.

Shalek, A.K., Satija, R., Adiconis, X., Gertner, R.S., Gaublomme, J.T., Raychowdhury, R., Schwartz, S., Yosef, N., Malboeuf, C., Lu, D., et al. (2013). Single-cell transcriptomics reveals bimodality in expression and splicing in immune cells. Nature *498*, 236–240.

Shalek, A.K., Satija, R., Shuga, J., Trombetta, J.J., Gennert, D., Lu, D., Chen, P., Gertner, R.S., Gaublomme, J.T., Yosef, N., et al. (2014). Single-cell RNA-seq reveals dynamic paracrine control of cellular variation. Nature *510*, 363–369.

Shin, J., Berg, D.A., Zhu, Y., Shin, J.Y., Song, J., Bonaguidi, M.A., Enikolopov, G., Nauen, D.W., Christian, K.M., Ming, G.-L., and Song, H. (2015). Single-cell RNA-seq with waterfall reveals molecular cascades underlying adult neurogenesis. Cell Stem Cell *17*, 360–372.

Snippert, H.J., van der Flier, L.G., Sato, T., van Es, J.H., van den Born, M., Kroon-Veenboer, C., Barker, N., Klein, A.M., van Rheenen, J., Simons, B.D., and Clevers, H. (2010). Intestinal crypt homeostasis results from neutral competition between symmetrically dividing Lgr5 stem cells. Cell *143*, 134–144.

Tabansky, I., Lenarcic, A., Draft, R.W., Loulier, K., Keskin, D.B., Rosains, J., Rivera-Feliciano, J., Lichtman, J.W., Livet, J., Stern, J.N.H., et al. (2013). Developmental bias in cleavage-stage mouse blastomeres. Curr. Biol. *23*, 21–31.

Teta, M., Rankin, M.M., Long, S.Y., Stein, G.M., and Kushner, J.A. (2007). Growth and regeneration of adult beta cells does not involve specialized pro- genitors. Dev. Cell *12*, 817–826.

Trapnell, C. (2015). Defining cell types and states with single-cell genomics. Genome Res. *25*, 1491–1498.

Treutlein, B., Brownfield, D.G., Wu, A.R., Neff, N.F., Mantalas, G.L., Espinoza, F.H., Desai, T.J., Krasnow, M.A., and Quake, S.R. (2014). Reconstructing lineage hierarchies of the distal lung epithelium using single-cell RNA-seq. Nature *509*, 371–375.

Uhlen, M., Fagerberg, L., Hallstrom, B.M., Lindskog, C., Oksvold, P., Mardinoglu, A., Sivertsson, A., Kampf, C., Sjostedt, E., Asplund, A., et al. (2015). Tissue-based map of the human proteome. Science *347*, 1260419.

Wang, B., Zhao, L., Fish, M., Logan, C.Y., and Nusse, R. (2015). Self-renewing diploid Axin2+ cells fuel homeostatic renewal of the liver. Nature *524*, 180–185.

Watanabe, K., Ueno, M., Kamiya, D., Nishiyama, A., Matsumura, M., Wataya, T., Takahashi, J.B., Nishikawa, S., Nishikawa, S.-I., Muguruma, K., and Sasai, Y. (2007). A ROCK inhibitor permits survival of dissociated human embryonic stem cells. Nat. Biotechnol. *25*, 681–686.

Yanger, K., and Stanger, B.Z. (2011). Facultative stem cells in liver and pancreas: fact and fancy. Dev. Dyn. *240*, 521–529.

Yanger, K., Knigin, D., Zong, Y., Maggs, L., Gu, G., Akiyama, H., Pikarsky, E., and Stanger, B.Z. (2014). Adult hepatocytes are generated by self-duplication rather than stem cell differentiation. Cell Stem Cell *15*, 340–349.

Ziv, O., Glaser, B., and Dor, Y. (2013). The plastic pancreas. Dev. Cell *26*, 3–7.